Multiple-robot drug delivery strategy through coordinated teams of microswimmers

U Kei Cheang, Kyoungwoo Lee, Anak Agung Julius, and Min Jun Kim

Citation: Applied Physics Letters **105**, 083705 (2014); doi: 10.1063/1.4893695
View online: http://dx.doi.org/10.1063/1.4893695
View Table of Contents: http://scitation.aip.org/content/aip/journal/apl/105/8?ver=pdfcov
Published by the AIP Publishing

Multiple-robot drug delivery strategy through coordinated teams of microswimmers

U Kei Cheang,[1] Kyoungwoo Lee,[2] Anak Agung Julius,[3] and Min Jun Kim[1,a)]
[1]*Department of Mechanical Engineering & Mechanics, Drexel University, Philadelphia, Pennsylvania 19104, USA*
[2]*Department of Computer Science, Yonsei University, Seoul 120-749, South Korea*
[3]*Department of Electrical, Computer and Systems Engineering, Rensselaer Polytechnic Institute, Troy, New York 12180, USA*

(Received 30 March 2014; accepted 10 August 2014; published online 29 August 2014)

Untethered robotic microswimmers are very promising to significantly improve various types of minimally invasive surgeries by offering high accuracy at extremely small scales. A prime example is drug delivery, for which a large number of microswimmers is required to deliver sufficient dosages to target sites. For this reason, the controllability of groups of microswimmers is essential. In this paper, we demonstrate simultaneous control of multiple geometrically similar but magnetically different microswimmers using a single global rotating magnetic field. By exploiting the differences in their magnetic properties, we triggered different swimming behaviors from the microswimmers by controlling the frequency and the strength of the global field, for example, one swim and the other does not while exposed to the same control input. Our results show that the balance between the applied magnetic torque and the hydrodynamic torque can be exploited for simultaneous control of two microswimmers to swim in opposite directions, with different velocities, and with similar velocities. This work will serve to establish important concepts for future developments of control systems to manipulate multiple magnetically actuated microswimmers and a step towards using swarms of microswimmers as viable workforces for complex operations. © *2014 AIP Publishing LLC*. [http://dx.doi.org/10.1063/1.4893695]

The revolutionary potential of micro/nanorobotics to significantly reduce the invasiveness of surgeries have facilitated many studies to improve localized drug delivery by providing the possibility for high controllability in directing drug load units to target specific individual cells and nowhere else.[1] Magnetic particles had been widely established as an effective material for robotic nanoparticle drug delivery methods, steered and pulled using magnetic gradients, they can enhance targeting capability over traditional methods of using enhanced permeability and retention (EPR) effect and targeting moieties.[2,3] However, the use of gradient force may be relatively ineffective against high drag force, especially in decreasing scales.[4,5] To enhance propulsion capabilities in small scales, many efforts followed Purcell's work on nonreciprocal swimming[1] to develop strategies for low Reynolds number locomotion by utilizing biologically inspired mechanisms such as the bacterium-like rotating helical microswimmers[6–10] and the sperm-like flexible microswimmers.[11,12] Other work, such as the electrically controlled microbiorobots,[13] magnetically steered ciliate protozoa,[14] chemically driven propellers,[15–20] optically deformed 3-bead systems,[21] bi-flagellated micro-objects,[22] demonstrated effective low Reynolds number propulsion; while helical micromachines,[6] sperm-driven microrobots,[23] microdrills,[24,25] and magnetic microrobots[26–28] demonstrated feasibility for biomedical applications such as minimally invasive surgeries (MIS), targeted localized drug delivery, and *in vitro* cell and tissue manipulation.

While these examples demonstrated low Reynolds number propulsion and performance of simple tasks, the idea of navigating *in vivo* for drug delivery have not been seriously considered. Realistically, a large number of microrobots are needed to carry the necessary dosage, but may result in a relative small percentage reaching the target.[29] This is due to cumbersome control caused by homogenous responses of robots under a global control signal and the inability to navigate dimensionally limited pathways, imposing external limitations that hinder the scalability of deployment number and drug dosage. To approach a feasible solution for drug delivery, multi-robot control must be implemented in order to effectively manipulate a large number of micro/nanorobots to target locations.

In a drug delivery scenario using multi-robot control, numerous coordinated teams of micro/nanorobots will approach the target in concert or separately and then converge and gather at a specific location to release the pharmaceutical payloads in order to enhance drug accumulation on small targets such as individual cells; this concept was demonstrated using live bacteria.[30] Recent work have demonstrated different strategies for multi-robot control and positioning; such as the stress-engineered MEMS microrobots driven using transition voltages,[31] the wireless resonant magnetic microactuators controlled through resonant frequencies,[32] the identical microrobots selectively positioned using specialized surfaces,[33] the heterogeneous magnetic microrobots manipulated in 3D using magnetic fields,[34,35] and the magnetotactic protozoan cells steered independently using single inputs.[36,37] The limitations of these strategies lies in their need for unique near- or on-surface microrobots

a)Electronic mail: mkim@coe.drexel.edu

or specialized test bed surfaces, which consequently narrow the range of potential applications. Here, we present a strategy to control multiple geometrically similar rotating magnetic microswimmers in bulk-fluid, for which each swimmer is given the same control input. This concept of multi-robot control capitalizes the microswimmers' magnetic heterogeneity, which is applicable not only to the three-bead microswimmers discussed in this paper but also to most rotating magnetic microswimmers such as the widely studied helical structured microswimmers.[6,7,9,10] Further, the inorganic nature of the applicable microswimmers allows for a wide range of operational environments such as various pH and ionic conditions. Also, biocompatible materials and coatings can be used.[27,38,39]

The microswimmer consists of three beads, forming an achiral structure with one plane of symmetry, hence the name *achiral microswimmer*. Upon actuation by a rotating field, the microswimmers produce propulsion by rotating about non-symmetrical axes (Fig. 1(a)). By controlling the field's frequency, strength, and direction, we manipulated the microswimmers' velocities, modes of motion, and heading direction, respectively. The mode of motion is defined as the rotation axis relative to the microswimmer's distance and orientation (Fig. 1(c) left), in other words, the swimming forms of the microswimmers. For multi-robot manipulation, two microswimmers with different magnetic properties will exhibit different modes of motion under a global field, thus a single control input will yield two different motions resulting in two distinctive velocities from the two microswimmers.

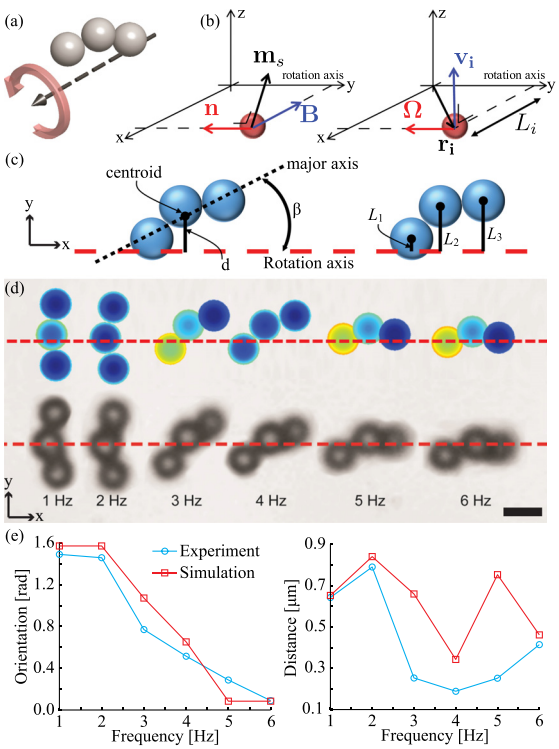

FIG. 1. (a) Schematic of an achiral microswimmer rotating about non-symmetrical axes to achieve propulsion. The dashed arrow line is the rotation axis, which also indicates the swimming direction. (b) Schematic for analyzing torque balance. (c) (Left) illustrations showing the parameters used for the characterization of rotation axis and (right) the distances of each beads from the rotation axis corresponding to $L_{1,2,3}$ from Eq. (3). (d) Qualitative comparison of the simulation prediction to the experimental characterization of the change in rotation axis. Scale bar is 5 μm. (e) Quantitative comparison of the orientation and the distance of centroid from the rotation axis.

Three-bead microswimmers were fabricated using three magnetic micro-particles (4.35 μm) linked together via biotin-streptavidin. The chemical binding helps overcome the linearity of magnetic self-assembly to form curved structures (Fig. 1). Magnetic beads (Spherotech) have iron oxide cores and are amino-coated. The beads were separated into two batches; one batch was mixed with 1 mg/ml of purified avidin protein and the other with 25 mg/ml *N*-hydroxysuccinimide-biotin, and subsequently incubated for 2 h. The batches are diluted using 30 mg/ml NaCl solution to 0.1 mg/ml to avoid aggregation and then combined in a reaction mix to yield three-beads microswimmers. Mixing introduces randomness to the process resulting in different structures; nonetheless, the three-bead structures can be easily obtained. Biotin-streptavidin linkage provides a very strong bonding,[40–42] ensuring structural perseveration under time-varying magnetic forces.

Under the low Reynolds number approximation, the two opposing angular torques, magnetic torque $\mathbf{T}_m$, and hydrodynamic torque $\mathbf{T}_r$, must counterbalance in order to achieve synchronous rotation between the microswimmer and the magnetic field at a steady angular velocity[43,44]

$$\mathbf{T}_m = -\mathbf{T}_r. \tag{1}$$

The magnetic torque is expressed as

$$\mathbf{T}_m = \mathbf{m}_s \times \mathbf{B},$$

where $\mathbf{m}_s$ is the magnetic moment vector of the microswimmer and $\mathbf{B}$ is the magnetic field vector. Fig. 1(b) illustrates our analysis for the magnetic torque $\mathbf{T}_m$ and hydrodynamic torque $\mathbf{T}_r$. As a three-bead magnetic chain, the magnetic torque of the microswimmer can be calculated as the sum of the torque exerted on each bead,[43–46] resulting in

$$\mathbf{T}_m = \frac{27\mu_0 m^2}{64\pi R^3}\sin(2\alpha)\,\mathbf{n},$$

where μ_0 is the permeability constant ($4\pi \times 10^{-7}$ T·m/A), R is the radius of the beads, m is the magnetic dipole induced by the $\mathbf{B}$ field, α is the phase lag angle, and $\mathbf{n}$ is the unit vector perpendicular $\mathbf{m}_s$ and $\mathbf{B}$ vectors. For steady synchronous rotation, the phase lag α should be less than $\pi/4$.[44]

The hydrodynamic torque due to rotational motion under stokes approximation is

$$\mathbf{T}_r = -\eta \mathbf{M}\boldsymbol{\Omega},$$

where η is the dynamic viscosity, $\mathbf{M}$ are the rotational resistance tensors, and $\boldsymbol{\Omega}$ are the rotational motion.[47] The torque $\mathbf{T}_r$ can be considered as the combined torque of the three individual beads revolving from the rotation axis.[48] The drag of i-th bead is modeled using Stoke's law

$$\mathbf{F}_{d,i} = -6\pi\eta R\mathbf{v}_i,$$

where $\mathbf{v}_i$ is the tangential velocity of the *i-th* bead. The hydrodynamic torque due to the drag of the *i-th* bead can be written as

$$\mathbf{T}_{r,i} = \mathbf{r}_i \times \mathbf{F}_{d,i}, \tag{2}$$

$$= -6\pi\eta R(\mathbf{r}_i \times \mathbf{v}_i), \tag{3}$$

where $\mathbf{r}_i$ is the vector position of the *i-th* bead. Taking the sum of the hydrodynamic torques from each of the three beads, we get

$$\begin{aligned}\mathbf{T}_r &= \mathbf{T}_{r,1} + \mathbf{T}_{r,2} + \mathbf{T}_{r,3},\\ &= -6\pi\eta R \sum_{i=1}^{3} \mathbf{r}_i \times \mathbf{v}_i,\\ &= -6\pi\eta R \sum_{i=1}^{3} \mathbf{r}_i \times (\mathbf{\Omega} \times \mathbf{r}_i).\end{aligned}$$

Denote

$$\mathbf{\Omega} = [-\omega, 0, 0]^T,$$

$$\mathbf{r}_i = [x_i, y_i, z_i]^T.$$

From here, it follows that

$$\mathbf{r}_i \times (\mathbf{\Omega} \times \mathbf{r}_i) = \omega[-y_i^2 - z_i^2, x_i y_i, x_i z_i]^T.$$

Therefore

$$\mathbf{T}_r = 6\pi\eta R\omega \left[\sum_{i=1}^{3} y_i^2 + z_i^2, \sum_{i=1}^{3} -x_i y_i, \sum_{i=1}^{3} -x_i z_i\right]^T.$$

Under the assumption of (1), the y and z components of $\mathbf{T}_r$ are zero. Therefore,

$$\mathbf{T}_r = 6\pi\eta R\omega[L_1^2 + L_2^2 + L_3^2, 0, 0]^T, \tag{4}$$

where

$$L_i = \sqrt{y_i^2 + z_i^2},$$

$$\mathbf{T_r} = -6\pi\eta R(L_1^2 + L_2^2 + L_3^2)\mathbf{\Omega}, \tag{5}$$

where $L_{1,2,3}$ are the beads' distances from the rotational axis (Fig. 1(c) right). The microswimmers were observed to be rigid; hence, the angular velocity $\mathbf{\Omega}$ is the same for all three beads.

Based on the torque balance (Eq. (1)), we experimentally characterized the changes to the rotation axis that will lead to different modes of motion by increasing the field's frequency (1–6 Hz) at a constant strength of 5.06 mT, which match favorably with our analytical prediction (Fig. 1(d)). Noted that the rotation axis changes in the body-fixed perspective; whereas in normal frame, the microswimmer's orientation changes. The angle between the major axis to the rotation axis, β, and centroid's distance from the rotation axis, d, were compared between the simulation and experiment (Fig. 1(c) left), where the discrepancies were less than 0.35 rad and 0.55 μm, respectively (Fig. 1(e) and Table I). The relationship in Eq. (1) depicts that $L_{1,2,3}$ in Eq. (5) must change in order to maintain torque balance; hence, the rotation axis will change accordingly given the microswimmer's structural constraints; likewise, the same will happen if frequency stays constant while field strength changes. The corresponding velocity profile (Fig. 2) categorized observable three modes of motion, (1) near-symmetrical rotation resulting in negligible propulsion, (2) non-symmetrical rotation resulting in non-reciprocal motion and active propulsion, and (3) wiggling motion resulting in negligible propulsion. The images in Fig. 2 show the trajectory of a representative microswimmer under the three modes of motion for 3 s. The wiggling motion is a result of the phase lag angle α being larger than $\pi/4$.

TABLE I. Value for L1, L2, and L3 for the simulation and experiment in Fig. 1(c).

		1 Hz	2 Hz	3 Hz	4 Hz	5 Hz	6 Hz
Experiment	L_1	3.84	3.60	2.40	1.76	0.80	0.16
	L_2	0.08	0.08	0.64	0.80	0.88	0.64
	L_3	−4.08	−4.16	−2.80	−2.00	−1.28	−0.48
Simulation	L_1	5.07	4.64	3.49	3.49	0.91	0.48
	L_2	0.87	0.44	2.18	2.18	1.74	1.31
	L_3	−3.33	−3.77	−1.05	−1.05	0.32	−0.12

For multi-robot control, geometrically similar microswimmers with distinctive magnetic properties were fabricated using two types of magnetically different beads of the same size (Spherotech AM-40–10 and AFM-40–10). Microswimmers with the same magnetic properties, fabricated with same type of magnetic beads, will respond similarly under a global magnetic field. However, with distinctive magnetic properties, the individual microswimmers will exhibit unique responses under a global rotating field, thereby leading to different swimming velocities, modes of motion, and directions. Additionally, geometrically dissimilar microswimmers can also be used as long as they possess

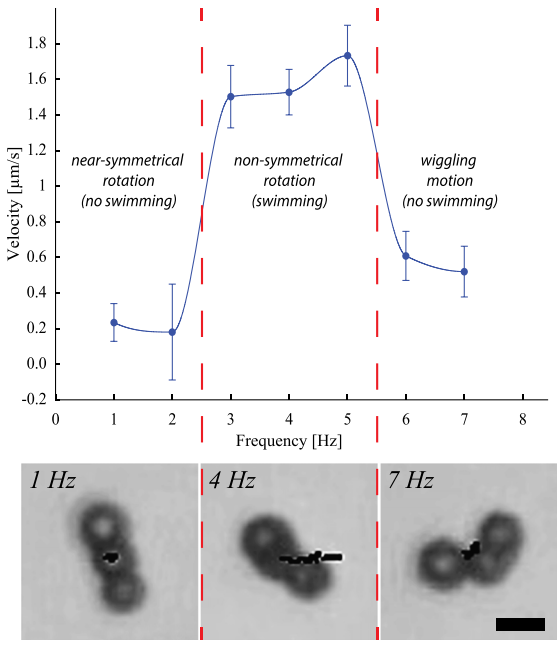

FIG. 2. Plot showing average speed of a microswimmer at various frequencies of the rotating field with a constant field strength. Under this condition, the microswimmer undergoes varying torque balance conditions resulting in different modes of motion. The error is from the pixel size of the camera and the time of observation. The images show the trajectories of the three modes of motions for 3 s. Scale bar is 5 μm. (Multimedia view) [URL: http://dx.doi.org/10.1063/1.4893695.1]

different magnetic properties, such as four beads or five beads; the possibility of which increases scalability and flexibility for different scenarios where different shapes of microswimmers are needed.

The field strength (mT), rotation direction (CW/CCW), and rotation frequency (Hz) of the magnetic field can be controlled through our magnetic control system (see supplementary material[49]). For *xy*-planar control, the resultant field can be expressed as

$$\mathbf{B} = B_0[\sin(\theta)\sin(\omega t), \quad \cos(\theta)\sin(\omega t), \quad \cos(\omega t)]^T, \quad (6)$$

which rotates with angular velocity ω around the unit vector

$$\mathbf{n} = [-\cos(\theta), \quad \sin(\theta), 0]^T, \quad (7)$$

which corresponds to the swimming direction, where B_0 is the amplitudes of the field generated by the *xyz* coils, ω is the rotational frequency, and θ is the rotation of the plane of the rotating field. For our approximate Helmholtz coil, the magnitude of the field B_0 of a pair of coils can be modeled as

$$B_0 = \frac{\mu_0 nIR_{coil}}{2\left(R_{coil}^2 + d^2 - 2Dd + D^2\right)^{3/2}} + \frac{\mu_0 nIR_{coil}}{2\left(R_{coil}^2 + d^2 + 2Dd + D^2\right)^{3/2}}, \quad (8)$$

where μ_0 is the permeability constant, n is the number of turns of the coils, I is the applied current, R_{coil} is the radius of the coils, D is the distance between a pair of coils, and d is the position between the coil. At the center of the coil, which is the position we are interested in, the position d is equal to zero. For more details on the approximate Helmholtz coil configuration, refer to Cheang *et al.*[8]

Using Eqs. (6)–(8), we fully manipulated the field's frequency, strength, and direction, which allow us to manipulate the torque balance and control the microswimmers' modes of motion as described in Fig. 2. Under nonsymmetrical rotation, as shown in Fig. 2, their velocity can be modulated linearly with rotation frequency, provided their rotation axis remains the same (Fig. 3). Through this, we can apply a global magnetic field on multiple magnetically different microswimmers and observed different swimming behaviors (velocity, direction, and mode of motion). In case of fluids with high viscosity, the only difference will be the required power to actuate the microswimmers since the magnetic torque is directly relates to the viscosity, as suggested in Eq. (5).

The microswimmers were transferred to a polydimethylsiloxane (PDMS) chamber (3 mm diameter, 2 mm height) and submerged in NaCl solution to increase buoyancy. The chamber was sealed to prevent evaporation and to minimize flow. The chamber was then placed inside the approximate Helmholtz coils for experiments.

We captured a 40 s video (63× magnification and 60 fps) showing three different scenarios, as representative results, where two microswimmers exhibited different speed and directions under a global magnetic field (see multimedia in Fig. 4). In each scenario, the control inputs, rotation

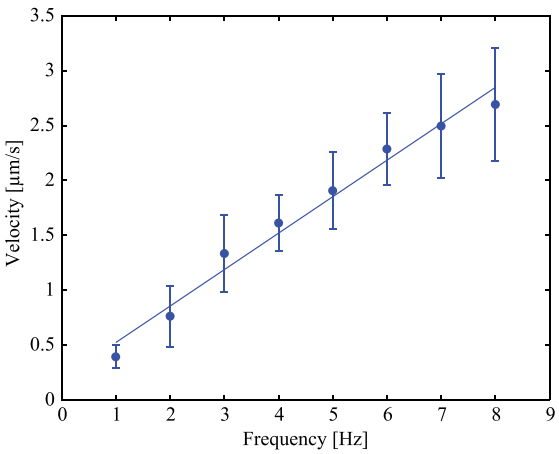

FIG. 3. Average swimming speed of four different microswimmers with increasing frequency, while maintaining a constant frequency to field strength ratio.

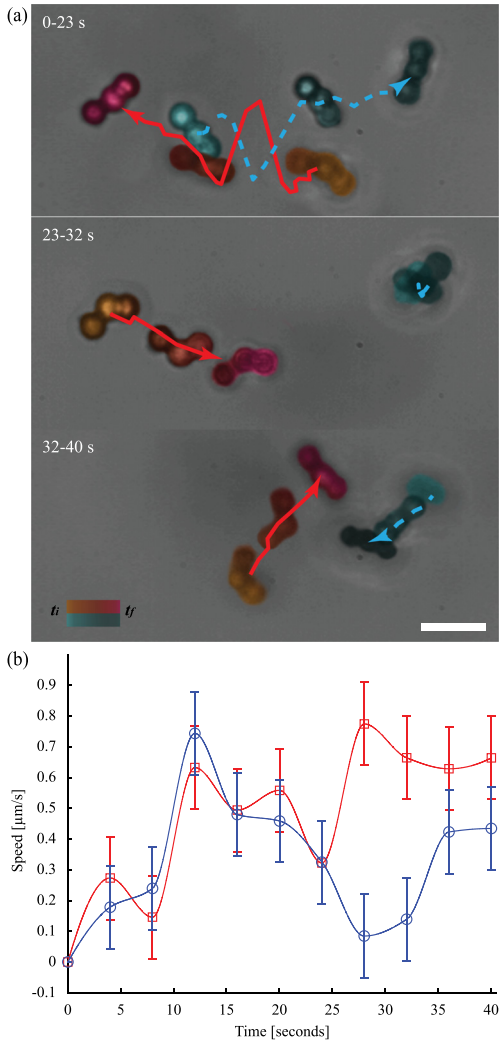

FIG. 4. (a) Experiment demonstrating control of two magnetically heterogeneous microswimmers (red and blue trajectories). The three images show different time intervals when the microswimmers exhibited different modes of motion. (Top) from 0 to 23 s, the two microswimmers swam in opposing directions with comparable velocities. (Middle) from 23 to 32 s, the red microswimmer swam to the right while the blue microswimmer showed no active propulsion. (Bottom) from 32 to 40 s, the microswimmers swam in opposing directions with different velocities. The scale bar is 10 μm. (b) Plot showing the average velocities of the two microswimmers in during the experiment. (Multimedia view) [URL: http://dx.doi.org/10.1063/1.4893695.2]

frequency, and field strength varied to trigger different modes of motions from the two microswimmers. In the first scenario, from 0 to 2 s, the two microswimmers swam in opposite directions with similar speed profiles, where the red (solid line trajectory) and blue (dotted line trajectory) microswimmers traveled at average speeds of 0.357 μm/s and 0.346 μm/s respectively (Fig. 4(a) top); the rotation frequency and field strength were 6 Hz and 2.315 mT, respectively. The opposite swimming directions are due to the handedness of the achiral structure, which is a result of the direction of the microswimmers' dipoles. The oscillation in the middle in Fig. 4(a), when the two crossed paths, was due to hydrodynamic interaction causing them to swirl around each other which corresponds to the peak speed at 12 s in Fig. 4(b). At around 23 s, both microswimmers stopped because no magnetic field was applied, demonstrating on/off control (not shown in Fig. 4, see multimedia in Fig. 4); the small observable speeds were due to diffusivity, unsteady fluid conditions, and small residual magnetic field from out of focused/view neighboring magnetized beads. In the second scenario, from 23 to 32 s, the red microswimmer swam to the right side at an average speed of 0.719 μm/s, while the blue microswimmer maintained near-stationary with an average speed of 0.112 μm/s (Fig. 4(a) middle). The frequency and field strength were 6 Hz and 1.8 mT, respectively. In the third scenario, from 32 to 40 s, the microswimmers swam in opposing directions where the red microswimmer swam at an average speed of 0.646 μm/s, while the blue microswimmer moved at a noticeably smaller average speed of 0.429 μm/s (Fig. 4(a) bottom). The rotation frequency and field strength were 6 Hz and 2.025 mT, respectively. Fig. 4(b) shows a plot of the speed profiles, measured every 4 s, of the two microswimmers for the full duration of the 40 s video. For all three scenarios, the ratio of rotation frequency and magnetic field strength was different; therefore, our experiment demonstrated manipulation of the microswimmers' modes of motion using the relationship established by the torque balance model to control multiple robotic microswimmers. Additional experiments had been performed to verify different modes of motion and swimming velocities of multiple microswimmers under a global field (see supplementary material[49]).

In conclusion, we have demonstrated a method to control multiple robotic microswimmers in bulk fluid using a global magnetic field by taking advantage of their magnetically heterogeneity. The achiral microswimmers were fabricated by conjugating three beads together using magnetic self-assembly and biotin-streptavidin linkage into arcs, where their magnetic properties can be made different by using two types of magnetic beads of the same size. Using analytical modeling and experimental characterization, we characterized their swimming behavior and developed a control scheme to simultaneously manipulate multiple units to exhibit different velocity and direction while given the same control input. This multi-robot manipulation strategy holds promise to address the some of the realistic challenges to utilize multiple units of micro/nanorobots for localized targeted operations, such as drug delivery.

This work was funded by National Science Foundation (CMMI 1000255) and Army Research Office (W911NF-11-1-0490) awards to M. J. Kim, by National Research Foundation of Korea (NRF) (2012-015421) award to K. Lee, by National Science Foundation (CMMI 1000284) award to A. A. Julius, and by National Science Foundation (NSF-GRF) award to U. K. Cheang.

[1]E. M. Purcell, Am. J. Phys. **45**, 3 (1977).
[2]C. Sun *et al.*, Adv. Drug Delivery Rev. **60**(11), 1252 (2008).
[3]J. Dobson, Drug Dev. Res. **67**(1), 55 (2006).
[4]J. J. Abbott *et al.*, Int. J. Rob. Res. **28**(11–12), 1434 (2009).
[5]P. Vartholomeos *et al.*, Annu. Rev. Biomed. Eng. **13**, 157 (2011).
[6]S. Tottori *et al.*, Adv. Mater. **24**(6), 811 (2012).
[7]A. Ghosh and P. Fischer, Nano Lett. **9**(6), 2243 (2009).
[8]U. K. Cheang *et al.*, Appl. Phys. Lett. **97**(21), 213704 (2010).
[9]F. Z. Temel and S. Yesilyurt, paper presented at the International Conference on Mechatronics, Istanbul, Turkey, 2011.
[10]K. E. Peyer *et al.*, Appl. Phys. Lett. **99**(17), 174101 (2011).
[11]R. Dreyfus *et al.*, Nature **437**, 862 (2005).
[12]W. Gao *et al.*, Small **8**(3), 460 (2012).
[13]E. B. Steager *et al.*, J. Micromech. Microeng. **21**(3), 035001 (2011).
[14]D. H. Kim *et al.*, Appl. Phys. Lett. **97**(17), 173702 (2010).
[15]K. M. Manesh *et al.*, ACS Nano **4**(4), 1799 (2010).
[16]A. A. Solovev *et al.*, Small **5**(14), 1688 (2009).
[17]Y. Hong *et al.*, Phys. Rev. Lett. **99**(17), 178103 (2007).
[18]W. Gao *et al.*, Small **9**(3), 467 (2013).
[19]T. Mirkovic *et al.*, ACS Nano **4**(4), 1782 (2010).
[20]W. Gao *et al.*, J. Am. Chem. Soc. **136**(6), 2276 (2014).
[21]M. Leoni *et al.*, Soft Matter **5**(2), 472 (2009).
[22]N. Mori *et al.*, Appl. Phys. Lett. **96**(8), 083701 (2010).
[23]V. Magdanz *et al.*, Adv. Mater. **25**(45), 6581 (2013).
[24]W. Xi *et al.*, Nanoscale **5**(4), 1294 (2013).
[25]A. A. Solovev *et al.*, ACS Nano **6**, 1751 (2012).
[26]S. Kim *et al.*, Adv. Mater. **25**, 5863 (2013).
[27]G. Dogangil *et al.*, paper presented at the IEEE International Conference on Intelligent Robots and Systems, Nice, France, 2008.
[28]S. Fusco *et al.*, Adv. Healthcare Mater. **2**(7), 1037 (2013).
[29]R. A. Freitas, J. Nanosci. Nanotechnol. **6**(9–10), 2769 (2006).
[30]D. de Lanauze *et al.*, Int. J. Rob. Res. **33**(3), 359 (2014).
[31]B. R. Donald *et al.*, J. Microelectromech. Syst. **17**(4), 789 (2008).
[32]D. R. Frutiger *et al.*, Int. J. Rob. Res. **29**(5), 613 (2010).
[33]C. Pawashe, S. Floyd, and M. Sitti, Appl. Phys. Lett. **94**(16), 164108 (2009).
[34]S. Floyd *et al.*, Int. J. Rob. Res. **30**(13), 1553 (2011).
[35]E. Diller, J. Giltinan, and M. Sitti, Int. J. Rob. Res. **32**(5), 614 (2013).
[36]A. Becker *et al.*, paper presented at the IEEE International Conference on Intelligent Robots and Systems, Tokyo, Japan, 2013.
[37]P. Kim *et al.*, paper presented at the International Conference on Ubiquitous Robots and Ambient Intelligence, Jeju, Republic of Korea, 2013.
[38]M. Mahmoudi *et al.*, Adv. Drug Delivery Rev. **63**(1), 24 (2011).
[39]H. Markides, M. Rotherham, and A. El Haj, J. Nanomater. **2012**, 1.
[40]J. Wong, A. Chilkoti, and V. T. Moy, Biomol. Eng. **16**(1), 45 (1999).
[41]E. P. Diamandis and T. K. Christopoulos, Clin. Chem. **37**(5), 625 (1991).
[42]K. K.-W. Lo *et al.*, J. Chin. Chem. Soc. **53**(1), 53 (2006).
[43]O. Sandre *et al.*, Phys. Rev. E **59**(2), 1736 (1999).
[44]S. L. Biswal and A. P. Gast, Phys. Rev. E **69**(4), 041406 (2004).
[45]C. Wilhelm *et al.*, Phys. Rev. E **67**(1), 011504 (2003).
[46]S. Melle *et al.*, Phys. Rev. E **61**(4), 4111 (2000).
[47]J. Happel and H. Brenner, *Low Reynolds Number Hydrodynamics: With Special Applications to Particulate Media* (Springer, 1965).
[48]M. Doi and S. F. Edwards, *The Theory of Polymer Dynamics* (Clarendon, Oxford, 1986).
[49]See supplementary material at http://dx.doi.org/10.1063/1.4893695 for details on magnetic control system and for video of multiple robot control of two microswimmers.